Spring 6-18-2018

Distribution and Localization of Novel Iodine Nanoparticles in the Human Glioma 1242 Growing in the Brains of Mice

Benjamin Billings
benjamin.billings@uconn.edu

Distribution and Localization of Novel Iodine Nanoparticles in the Human Glioma 1242 Growing in the Brains of Mice

By: Benjamin Billings
Advisor: Henry Smilowitz, PhD, UConn Health - Department of Cell Biology

Table of Contents

I. Abstract:

Observing and designing the *in vivo* distribution and localization of therapeutic nanoparticles is an essential aspect of developing and understanding novel nanoparticle-based medical treatments. This study investigates novel PEGylated Iodine-based nanoparticles (INPs), an alternate composition to the more widely researched gold nanoparticles (AuNPs), which may help avoid adverse effects associated with AuNPs, such as potential toxicity and skin discoloration, when used in similar applications. Determining the localization of the novel INPs within murine brains containing human glioma U-1242MG cells is critical in assisting the development of radiation dose enhancement therapy for this aggressive cancer. Radiation dose enhancement utilizes the increased radiation absorption of the INPs and subsequent increased electron and photon scattering to increase the therapeutic effect and possibly help reduce the radiation dose administered. This study serves to qualitatively and semi-quantitatively determine the distribution of the novel INPs within the murine brain, the tumor region, and at the cellular level within the tumor. This is accomplished through immunofluorescence staining and light and confocal microscopy, probing for CD31 (PECAM1), an endothelial cell marker, poly(ethylene glycol) (PEG), a nanoparticle marker, DAPI, a nucleus marker, and tdTomato, a fluorescent protein expressed by the implanted U-1242MG cells. The imaging at 10X and 63X magnification yielded evidence that the PEGylated INPs are distributed in and around the tumor to a much greater extent than elsewhere in the brain and there is some propensity for the INPs to localize in the vasculature far from the tumor region as well as within the tumor region. At the cellular level the INPs are not regularly taken up by cells and introduced into the cytoplasm within 24 hours of the last injection. Therefore, this study is relevant to radiation therapy in that it further characterizes the behavior of INPs in glioma containing murine brains, and from the data on where these particles exist, researchers can eventually develop a correlation of therapy results with INP localization at the cellular level to better develop patient treatments.

II. Introduction:

Radiation Dose Enhancement:

Radiation therapy is a fundamental element in the treatment of brain tumors and is frequently used in conjunction with surgical excision and chemotherapy. In regards to glioblastoma multiforme (GBM), radiotherapy is considered the standard of care when combined with the chemotherapeutic temozolomide [1]. In fact, radiation therapy has the potential to be useful as a curative treatment method in 25 % of all new cancer cases, and as palliative care in an additional 25 % of new diagnoses [2]. Nonetheless, though radiation therapy can kill malignant cells, and slow or halt the growth of tumors, by inducing DNA damage which interrupts the cellular division process ultimately leading to apoptosis or latency [3], it can also damage or kill healthy brain tissue and ultimately lead to radiation necrosis [2, 4, 5]. Radiation necrosis, which is essentially healthy brain tissue death following radiation therapy, often appears 6 months to 2 years after treatment due to the delayed cellular response to DNA damage acquired during radiation therapy in healthy tissues [4]. In particular, the endothelial cells of smaller blood vessels are most often affected and their death recruits lymphocytes and macrophages, which in turn trigger a cascade of cytokine activity and an inflammatory immune response. Ultimately, the inflammation induces new, though irregular vascular growth very prone to thrombosis and hemorrhage, leading to ischemic injury in healthy brain tissues [4]. Additionally, there are significant side effects associated with radiation necrosis including headache, drowsiness, memory loss, personality change, seizures, and even eventual death, while there are few well-studied treatment options for the condition [4].

One possible approach under development to mitigate the damage to healthy tissue is the use of heavy-atom-based nanoparticles to amplify radiation doses within tumors while delivering a less toxic dose to normal tissues [6, 7, 8, 9]. If heavy-atom based nanoparticles are loaded into tumors by any means, radiation dose enhancement is possible due to the increased absorbance of X-rays and subsequent increase in scattered electrons, ions, radicals, and other reactive chemical species in tissues due to the higher concentrations of heavy atoms present in the tumor [6]. Therefore, by exploiting the enhanced permeability and retention (EPR) effect of nanoparticles within tumors due to the malformed and leaky vasculature present in some tumors, nanoparticles can be distributed throughout a tumor by minimally invasive intravenous injection [10]. Thus, as researchers have shown dose enhancement with gold nanoparticles or iodine contrast media [6, 7, 8, 9], our lab seeks to demonstrate radiation dose enhancement with novel, PEGylated iodine-based nanoparticles. The INPs have the potential to avoid the renal toxicity of iodinated molecules [11] and the various disadvantages of gold nanoparticles including discoloration of the skin and the possibility of toxicity of gold nanoparticles presented in some studies but not in others [reviewed in 12].

a. PEGylation of Nanoparticles:

Due to the small size and high surface area to volume ratio of nanoparticles, there is a substantial fraction of the total number of atoms of the nanoparticles at the surface, with uncoordinated bonds. This results in a very high surface energy for small particles and the subsequent aggregation and adsorption of other nanoparticles and molecules in order to reduce the fraction of atoms with “dangling bonds”, and therefore reduce the overall surface energy. In order to mitigate this effect and retain nanoparticle size, ligands are often attached

to nanoparticles to resist protein adsorption and particle aggregation in an *in vivo* environment. The industry standard ligand that has emerged for this function has been poly(ethylene glycol) (PEG), a polyether which has been shown to be hydrophilic and bioinert [14, 16]. These properties, as well as the polymer's size allow particles with attached PEG ligands to increase their solubility and hydrodynamic size by increasing the amount of coordination sites for the aqueous solvation layer, allowing the avoidance of renal clearance, and a subsequent increase in circulation time [15]. Likewise, the bioinert behavior of PEG allows it to be used as a "stealth" agent on nanoparticles and other molecules, allowing PEGylated particles to avoid the immune system response as well as non-specific cellular uptake mostly by the reticuloendothelial system of the liver (RES), further increasing the circulation time [14, 15, 17]. This "stealth" effect is possible because the hydrophilic polymers resist opsonin binding, therefore resulting in fewer nanoparticles marked for endocytosis [18]. With enhanced circulation times, more drugs or nanoparticles are capable of being dispersed or deposited in the desired location, selected for by additional specific surface protein binding ligands or in the case of some tumors, the already existing, leaky vasculature, which enables blood borne molecules to enter the tumor interstitium [19, 20].

The novel iodine-based nanoparticles used in this study have been PEGylated to exploit the same phenomena mentioned above. Further, the PEG ligands are the molecules that are probed for with immunofluorescence imaging to determine the localization of the nanoparticles.

b. Human Glioma U-1242MG:

The model cell strain used in this experiment was U-1242MG, a human glioma. As a glioma, or a cancer arising from the glial cells of the brain, these cells are adapted to living in

brain tissue and thus are capable of rapid growth and invasion of healthy tissue. These tumors, referred to as glioblastomas when displaying highly invasive and proliferative behavior, are noted for having hyperplastic blood supplies as well. It is worth noting that due to the ability and tendency of U-1242MG cells to grow amongst healthy brain tissue, symptoms are not generally observed until the tumor is already quite large [21].

In this study, the implanted U-1242MG cells were transduced by Northwestern University to express the protein firefly luciferase as well as the fluorescent protein tdTomato. Hence the tumor could be monitored while growing with bioluminescence and viewed histologically by fluorescent microscopy.

c. Previous Research and Results

There have been several studies concerning the localization of PEGylated nanoparticles, including gold-based and polymer-based nanoparticles [22, 23]. The localization on the intercellular and intracellular level is ultimately dependent on the specific uptake proteins ligated to the nanoparticles as well as the final diameter of the nanoparticles [22]. In particular, the findings reported concerning PEGylated gold nanoparticles (AuNPs) stated that 2.4 nm AuNPs localized in the nucleus once internalized, 5.5 – 8.2 nm AuNPs localized in the cytoplasm, and nanoparticles greater than 16 nm in diameter were not permitted into the cells and localized at the cellular periphery [22]. This study aims to characterize and compare the localization of the novel INPs with the results in these findings since there are similarities in the PEG nanoparticle surface, but differences in the core composition. Lastly, the novel INPs do not have specific cellular uptake proteins attached and therefore will not extensively use receptor-mediated endocytosis.

III. Materials & Methods:

a. Materials:

- Implantation
  - 8 week old, female, athymic nude mice; n = 3
  - U-1242MG cells expressing tdTomato fluorescent protein
  - 1-microliter syringe
  - Drill
  - Scalpel
  - Surgical Glue
  - Ketamine/Xylazine anaesthetic
  - Alcohol swabs, Betadine, Gauze pads
- Injection
  - PEGylated Iodine-based nanoparticles (INP)
  - 25 gauge syringe
  - Tail vein mouse restrainer
- Sectioning
  - Cryomatrix
  - Glass microscope slides
  - Pink slide tape/Japanese tape
  - Leica CM3050 S Research Cryostat
- Staining
  - Primary Antibodies
    - Goat-anti-Mouse/Rat CD31 diluted 1:100 in 1% BSA solution from R&D AF3628
    - Rabbit-anti-PEG diluted 1:500 in 1% BSA solution from Abcam ab51257
  - Secondary Antibodies
    - Donkey-anti-Rabbit conjugated with Alexa Fluor 488 diluted 1:400 in 1% BSA solution from Invitrogen a21206
    - Donkey-anti-Goat conjugated with Alexa Fluor 647 diluted 1:200 in 1% BSA solution from Life Technologies a21447
  - Solutions
    - Washing solution (phosphate-buffered saline (PBS))
    - Blocking Solution (1:10 dilution of PowerBlock in PBS)
    - Antibody Diluent (1% Bovine Serum Albumin in PBS)

        - Coverslip Mounting Solution (1:1000 Hoescht 33342 in 50% v/v Glycerol in PBS)
      - Coplin Jars
      - 1000 microliter, 100 microliter, 20 microliter, and 5 microliter micropipettes
    - Imaging
      - Fluorescence Light Microscope – Zeiss Axio Observer Z1
      - Confocal Microscope – Zeiss LSM 880
      - Zen Black/Zen Blue imaging software & Fiji image processing software

b. Methods:

Implantation of the human glioma U-1242MG cells into the brains of three, 8 week old, female, athymic, nude mice: Mice were sedated with an intraperitoneal injection of the ketamine/xylazine drug cocktail of approximately 90 mg/kg and 5 mg/kg dosages respectively. Upon complete sedation determined by the lack of a pedal or toe pinch reflex, a dorsal incision was made on each mouse's head to reveal the skull beneath. Next, with the 450-micrometer micro-drill, a hole was made through each skull and dura revealing the left hemisphere of the brain. A 27 gauge needle fitted with a 2.5 – 3 mm plastic, depth limiting collar connected to a 1-microliter syringe previously loaded with ~100,000 U-1242MG cells was then introduced carefully into each opening. The cells were then injected over the course of 1 minute and a total volume of 1 microliter. One minute later the needle was then removed and the skin was sutured using surgical glue to close the incisions.

Tumor Monitoring and INP Administration: The implanted tumors were then monitored using the In Vitro Imaging System (IVIS) Spectrum machine for 2-3 weeks to track tumor growth. After successful tumor growth indicated by a set signal threshold from the tumor, the mice were then injected 4 times with INP at 1.75 g I/kg body weight over 48 hours, with two injections 3 hours apart on two consecutive days. 24 hours

following the final injection the mice were deeply anesthetized and subjected to perfusion fixation.

Perfusion Fixation and Tissue Harvesting: Each mouse was anesthetized with the same surgical dose of the ketamine/xylazine cocktail described previously and monitored using the to pinch method for full anesthesia. Upon full anesthesia, each mouse was secured on its back with its limbs spread away from its body. A transverse incision was made through the skin of the abdomen followed by the muscle layer into the abdominal cavity of the mouse, careful to avoid any internal organs. Next, curved, blunt scissors were used to cut the ribs from the lateral incision toward the collarbone on each side. Tissue connecting the heart to the sternum was carefully trimmed away allowing for the rib cage to be held in place over the animal's head using a hemostat. A 15 gauge blunt needle was then introduced through the left ventricle into the ascending aorta and the right atrium was cut to allow for blood to drain from the circulatory system. Immediately following the laceration of the atrium, PBS was delivered through the needle for approximately 10 – 15 seconds followed by 10% formalin. This fluid was administered until the mouse was fully stiff and no further blood drained from the atrium. The brains were then harvested by resecting the skull and stored for 24 hours in a 10% formalin solution at 4° C. The brains were transferred to a 30% sucrose solution overnight at 4° C. Finally, the brains were cut laterally, mid-tumor and were submerged in Cryomatrix and frozen in dry ice cooled isopentane.

Cryosectioning: Once the blocks were prepared, microscope slide sections were prepared using the Leica CM3050 S Research Cryostat. A selected block was mounted onto a chilled pedestal, and aligned with the blade of the machine to ensure consistent

and level 7-micrometer sections with every cut. For each specimen sample, a section of microscope slide tape was applied to the mounted block and firmly secured with the use of a roller. The sample was then taken and quickly transferred to a chilled glass microscope slide. This process was repeated for the desired number of sections from various regions of the brains. The samples were then cross-linked to the slides with UV light.

Immunofluorescence Staining: Enough sections were taken to provide a series of controls for the staining protocol. This included sections stained with no antibodies, only primary antibodies, only secondary antibodies, individual combinations of primary and secondary, and all antibodies. Previous work in our lab has ruled out any non-exclusive and undesired antibody-antibody interactions as well as non-specific antigen labeling when using this specific set of antibodies. However, an isotype antibody control was not performed followed by a secondary antibody to determine the presence of any background signal. The same staining protocol was used for all slides and all antibody combinations and is described below.

All slides were placed in Coplin jars and rehydrated in PBS for 10 minutes. The slides were then removed and dried with Kimwipes, avoiding contact with any tissue on the slide. Next, each section was blocked using 100 microliters of the blocking solution, applied with a 100-microliter micropipette, ensuring full coverage of each individual section, avoiding tissue contact with the pipette. After 30 minutes, the blocking solution was removed by tilting each slide perpendicular to the work surface and tapping gently to dislodge the liquid. The slides were then placed back in the Coplin jars and washed in PBS for 5 minutes to remove any excess blocking solution. The slides were then

removed, dried, and prepared for the primary antibody addition. First, the primary antibody solution containing both primary antibodies was prepared in the proper dilution ratio for each antibody. Each section was then stained according to its series designation with approximately 80 microliters of its given antibody solution. To sections serving as controls and receiving neither of the two primary antibodies, a 1% BSA solution was applied. All slides were then incubated overnight at 4°C in a humidified environment.

Following the primary antibody incubation, the antibody solutions were removed and the slides were placed in Coplin jars and washed in PBS 3 times for 5 minutes each and then dried as described above. Similarly, one solution was prepared containing both secondary antibodies in their proper dilution ratios. Each section was then stained according to its series designation, again with approximately 80 microliters of staining solution. To sections receiving neither of the two secondary antibodies, 1% BSA in PBS was applied. The slides were then placed in a humidified environment and allowed to incubate at room temperature for 60 minutes. The slides were the washed 3 times in PBS for 5 minutes each wash and then dried and prepared for coverslip mounting.

The coverslip mounting media was prepared by adding 500 microliters of glycerol to 500 microliters of PBS in a 3 mL microcentrifuge tube. This solution was thoroughly mixed using a test tube vortex mixer. One microliter of the Hoescht 33342 stain was then added to the glycerol-PBS mixture and the solution was mixed using the vortex mixer again. Finally, using a 20-microliter micropipette, about 6 to 8 microliters of the prepared coverslip mounting media was applied to each section. A glass coverslip was then slowly lowered onto each slide taking care to trap as few air bubbles as possible. Lastly, using Kimwipes, any excess mounting media was removed by gently patting the edges of each

slide, taking care to not smudge or smear any solution across either glass surface. The prepared slides were then stored at -20°C in sealed container until they were imaged.

Fluorescence Imaging: All imaging was performed using either the Zeiss Axio Observer Z1 fluorescence light microscope or the Zeiss LSM 880 confocal microscope and images were processed using the Zen Blue software and the open-source software variant of ImageJ called Fiji. Images were taken in several formats including 10X magnification tile-scans and 20X magnification single frame images using the Zeiss Axio Observer Z1, and 63X magnification single frame images and 63X magnification z-stacks using the Zeiss LSM 880 confocal microscope.

IV. Results:

a. 10X Magnification Tile Scan:

In order to investigate the general localization of the novel INP, a tile-scan of the entire brain section containing the tumor region in the left hemisphere with a tumor free right hemisphere was taken on the Zeiss Axio Observer Z1. This tile-scan, conducted at 10X magnification, allowed moderate resolution over the entire surface with a white arrow indicating the center of the main tumor mass. The images demonstrated a much greater PEG signal in the hemisphere with implanted U-1242MG cells, as is evident in **Figure 1d**. Additionally, an overall increase in CD31 signal was obtained in and around the tumor region (**Figure 1c**).

In the region of interests marked in colored boxes in **Figure 1b**, the tile scan image is utilized to determine if the localization of PEG occurs at sites exhibiting CD31 signals. In the first region of interest marked by the red box in **Figure 1b**, an area lying along the midline of the brain far from the tumor, there is a strong correlation of PEG and CD31 signal, with little PEG signal outside of the regions exhibiting CD31 signal. This is

evident in **Figure 2**, and further in **Figure 3**, which shows the PEG stain more completely mapping the small vessels in the brain than the CD31 stain. This might be possible because more PEG molecules were trapped and exposed to the immunostaining antibodies than CD31 molecules, which are present at the intercellular junction sites, which may not all be exposed to the surface, or it is possible the antibody binding affinity of PEG is greater than that of CD31, thus increasing the fluorescent signal possible.

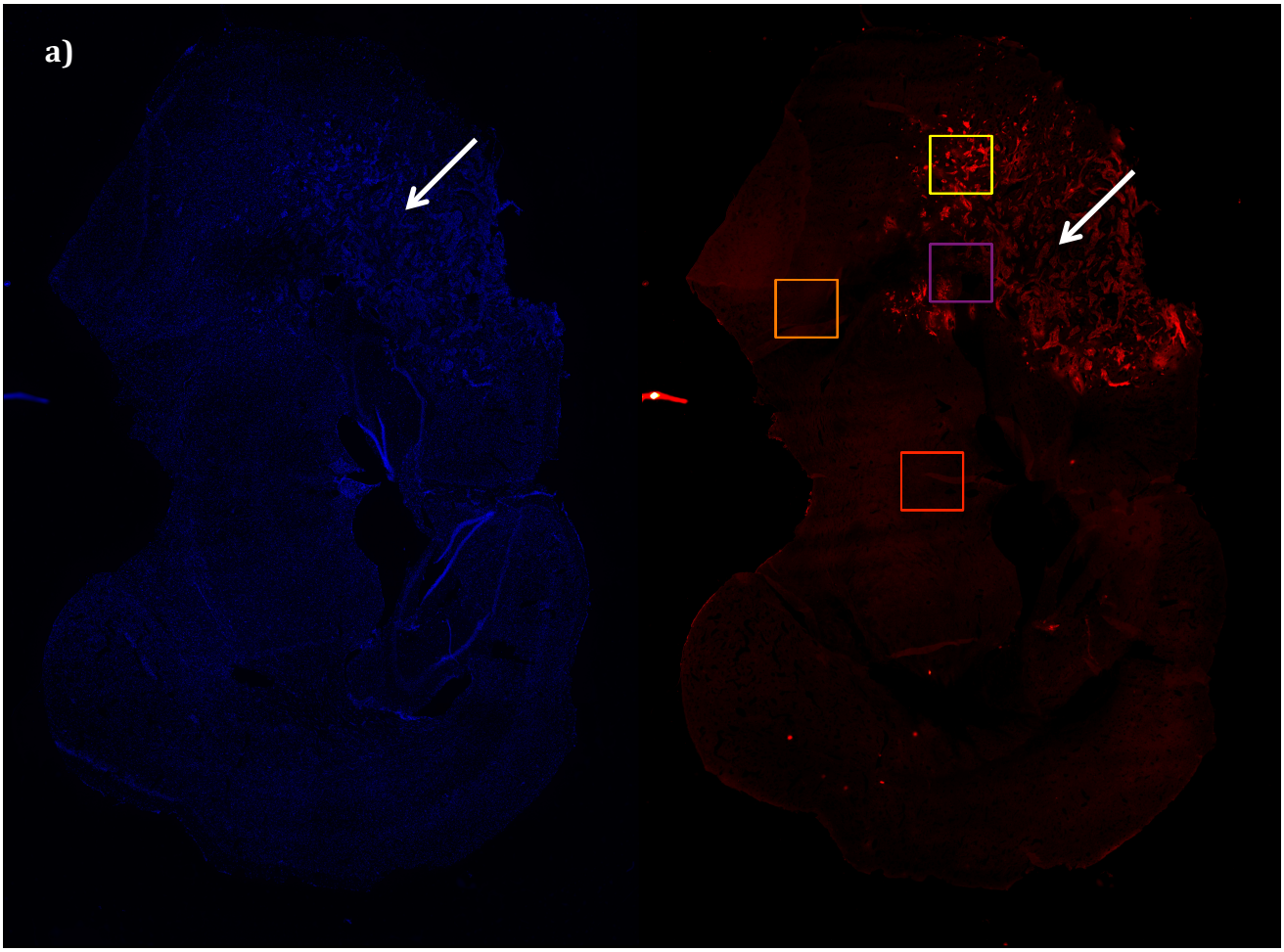

Figure 1a & 1b: 10X Tile Scan of murine brain with tumor present as well as INP. The image shows nuclei colored blue (a), U-1242MG cells colored red (b), endothelial cell marker CD31 colored cyan (c), and PEG colored green (d). The white arrow points to the center of the tumor.

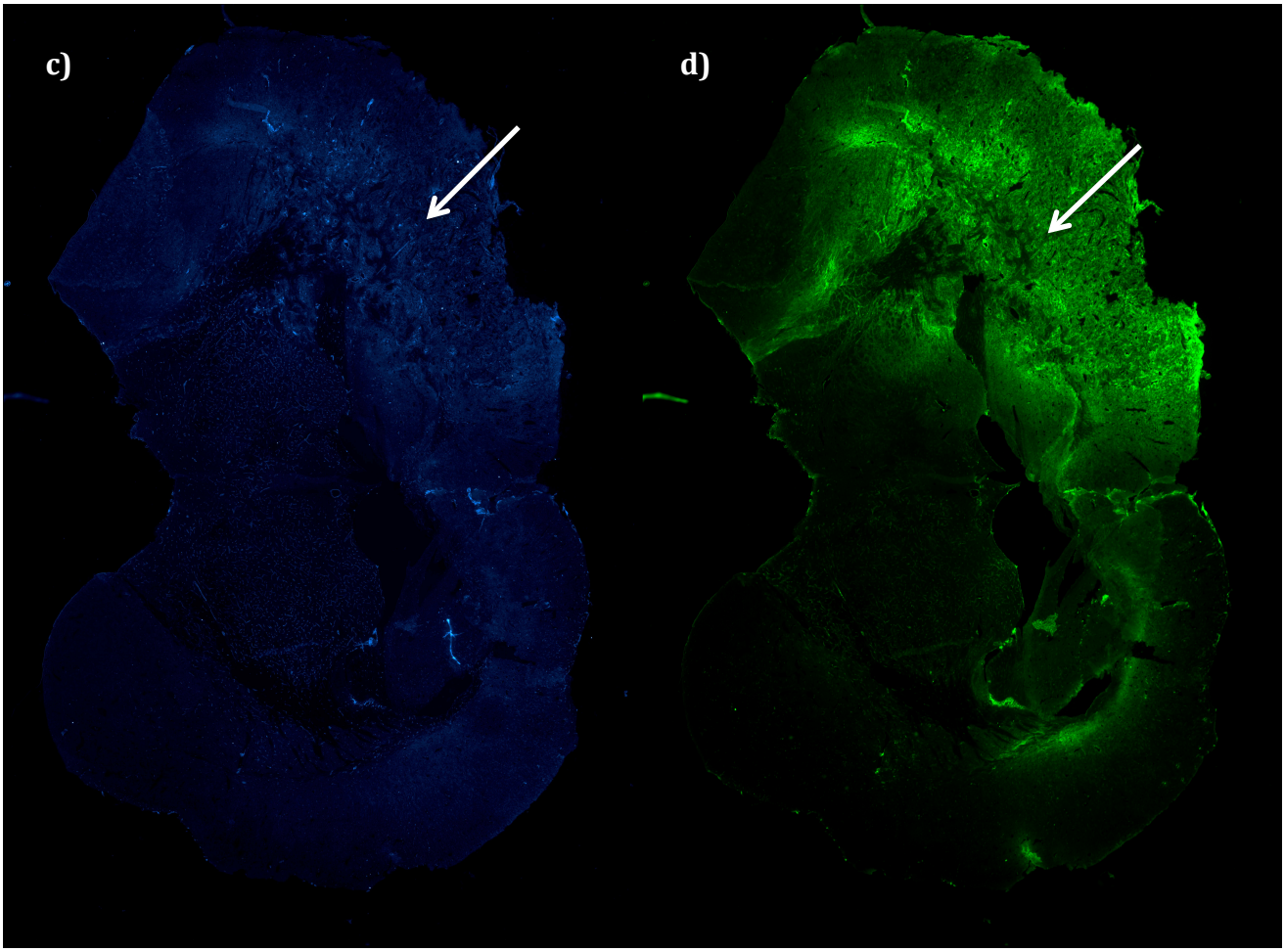

Figure 1c & 1d: 10X Tile Scan of murine brain with tumor present as well as INP. The image shows nuclei colored blue (a), U-1242MG cells colored red (b), endothelial cell marker CD31 colored cyan (c), and PEG colored green (d). The white arrow points to the center of the tumor.

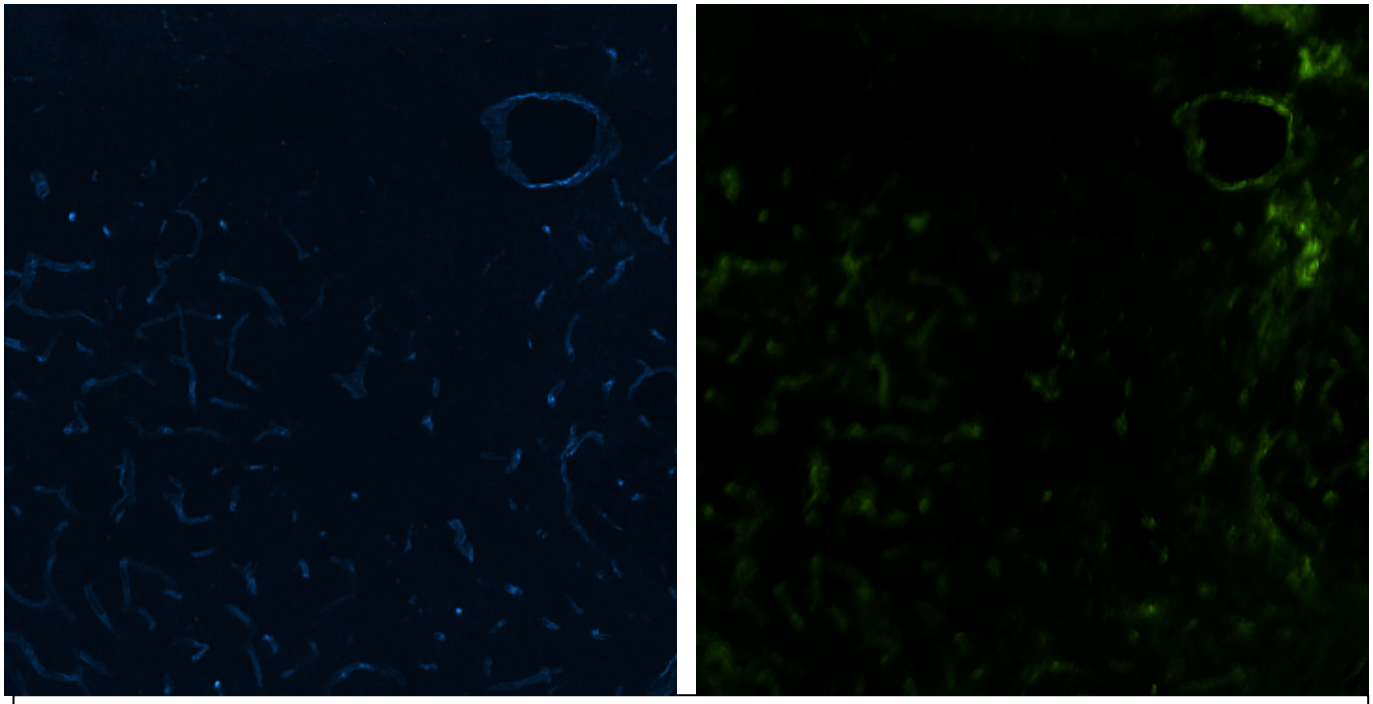

Figure 2: Region of interest 1 (red box in **Figure 1c**) outside of the tumor showing localization of PEG (right) in regions with CD31 endothelial marker staining (left). The channels for the U-1242MG cells and the cell nuclei stains were omitted because there was no tumor signal and cell nuclei were uniformly present at this magnification.

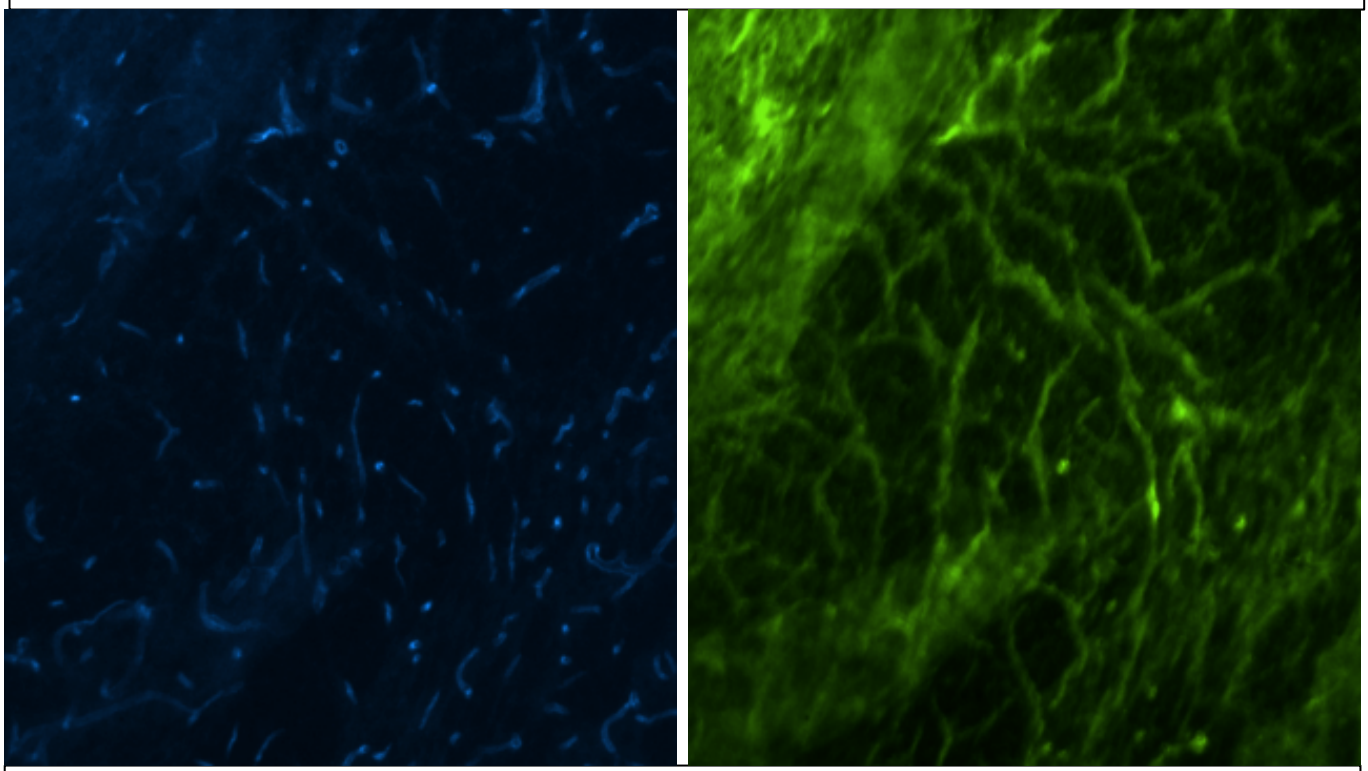

Figure 3: Region of interest 2 outside of the tumor (orange box) showing PEG (right) and CD31 (left) co-localization. In fact, in this image, the anti-PEG staining seems to map the vasculature of the section better than the CD31 staining, likely due to the much higher concentration of PEG antigens and subsequent contrast of the PEG stain.

In **Figures 4 & 5** regions of interest within the tumor were explored using 10X magnification to determine any correlation of PEG localization with CD31 expression within the tumor region, as well as in relation to tdTomato expressing U-1242MG cells and non-expressing native tissues. As is evident in **Figure 4**, there is a large signal indicating near uniform PEG distribution throughout the tumor, among both cancerous and non-cancerous cells. Likewise, in **Figure 5** several large vessels are clearly present, formed within tumor cell clusters, and exhibiting significant signal from both CD31 and PEG staining. Additionally, **Figure 6** shows a 10X magnification image with CD31, PEG, nuclei, and U-1242MG cells individually and overlaid. The result is a clear display of a high amount of CD31 antigens, a near uniform distribution of cell nuclei, a heterogeneous distribution of U-1242MG cells, displaying the invasive nature of this strain, and a near uniform distribution of PEG throughout this region. Nonetheless, the localization of the PEG is not clear at 10X magnification at the cellular level.

In order to address the ambiguity of the localization of the PEG signals at 10X magnification, a series of z-stack confocal microscopy images were taken on the Zeiss LSM 880 microscope at 63X magnification. **Figure 7** displays 3 levels of the stack selected to display a change in the PEG signal as the plane of focus proceeded into the center of a layer of cells. Additionally, in **Figure 7** a region of interest containing a strong signal for CD31 and PEG is highlighted. From this series it appears that the PEG signal is strongest at the surface and exterior of cells as well as in vessels and voids within the tissue. As this z-stack proceeded, the PEG signal further decreased, appearing only along the edges before increasing much like the top plane. A possible explanation for this behavior is the inability for the antibodies to effectively penetrate and stain intracellular PEG, which would alternatively explain why the PEG was not

seen localized in the cells, however as discussed later a membrane permeabilizer used in a staining protocol may confirm or deny this theory.

Finally, a quantitative analysis of the colocalization of the different signals was performed using the Pearson's Correlation Coefficient (PCC). This scale disregards signal intensity and simply compares signal presence at the same pixels in an image over different channels. The scale is from -1 to 1, with -1 signifying perfect antilocalization, 0 signifying no correlation, and 1 signifying perfect correlation. Using **Figure 6**, it was found within the tumor there was a PCC of -0.01 between the tumor cells and the PEG signal, indicating no specificity, and a PCC of 0.3 between the PEG and CD31 signals, indicating low to moderate colocalization specificity. Additionally, the PEG and CD31 PCC values were calculated for **Figures 2 through 5** to determine the colocalization propensity of PEG with CD31. PCC values outside the tumor in the regions of interest were 0.47 and 0.63 for **Figure 2 and 3** respectively, indicating moderate colocalization. PCC values within the tumor in the regions of interest displayed in **Figures 4 and 5** were 0.75 and 0.65 respectively indicating a strong correlation between the localization of CD31 and PEG signals. At 63X using **Figure 7** the PCC value between PEG and CD31 was 0.42, the PCC value between PEG and tdTomato was 0.05, and the PCC between PEG and nuclei was -0.10. It should be noted that the slight background present in these images is considered using the PCC metric, and the backgrounds of tdTomato was significant, bringing the PCC between PEG and tdTomato closer to 0. The results are summarized in the bar graph at the end of the results section.

Lastly, several calculations were done using **Figure 1** to determine the fractional area occupied by the tumor and the fraction of the PEG signal this area contained. Ultimately the tumor occupied about 16.5 percent of the sectional area and contained approximately 40 percent

of the PEG signal. This demonstrates the EPR effect and that PEG is loaded in the tumors more than outside of the tumor region. However, it also shows that about 60 percent of the signal related to PEG occurs outside the tumor region.

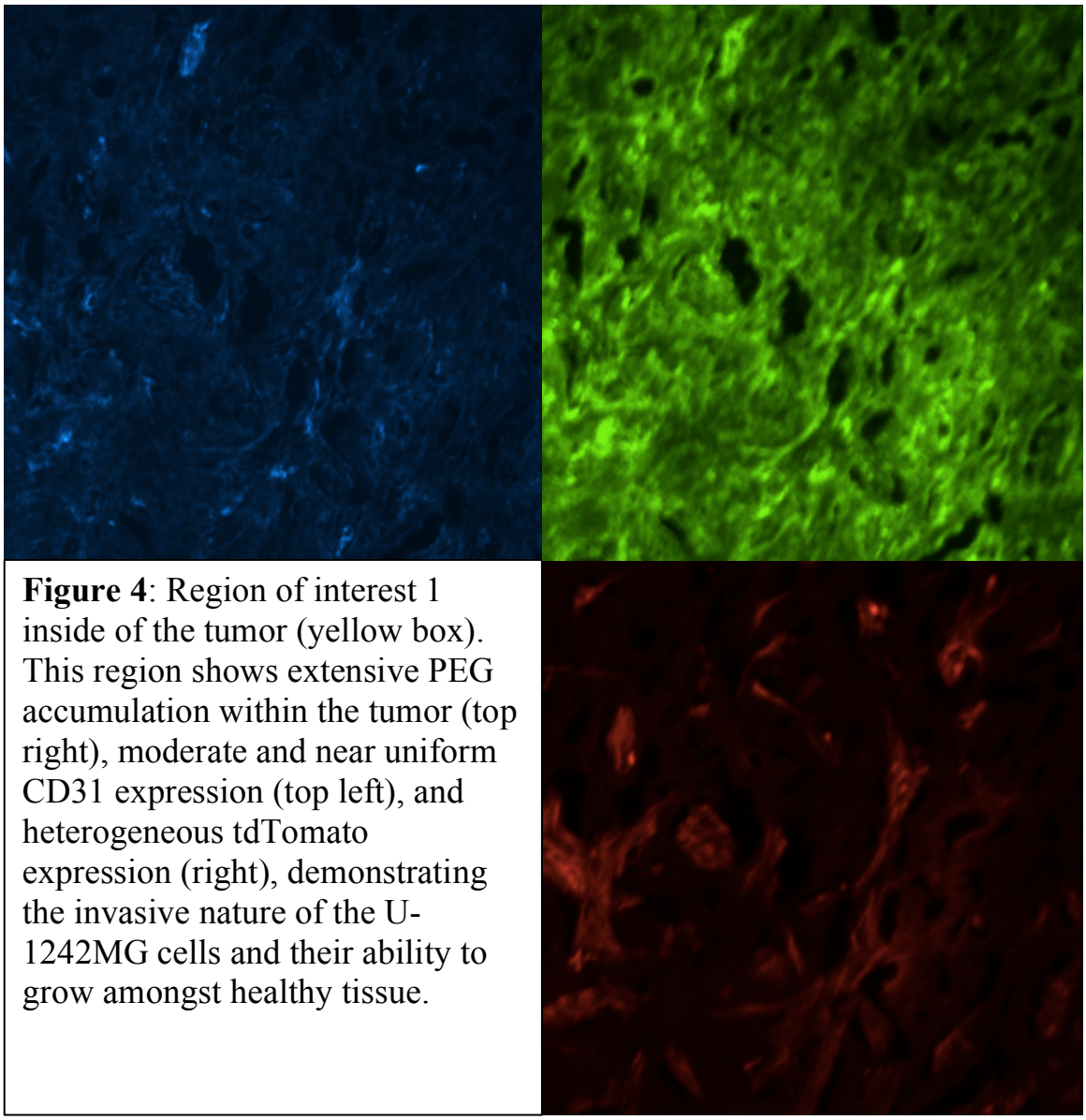

Figure 4: Region of interest 1 inside of the tumor (yellow box). This region shows extensive PEG accumulation within the tumor (top right), moderate and near uniform CD31 expression (top left), and heterogeneous tdTomato expression (right), demonstrating the invasive nature of the U-1242MG cells and their ability to grow amongst healthy tissue.

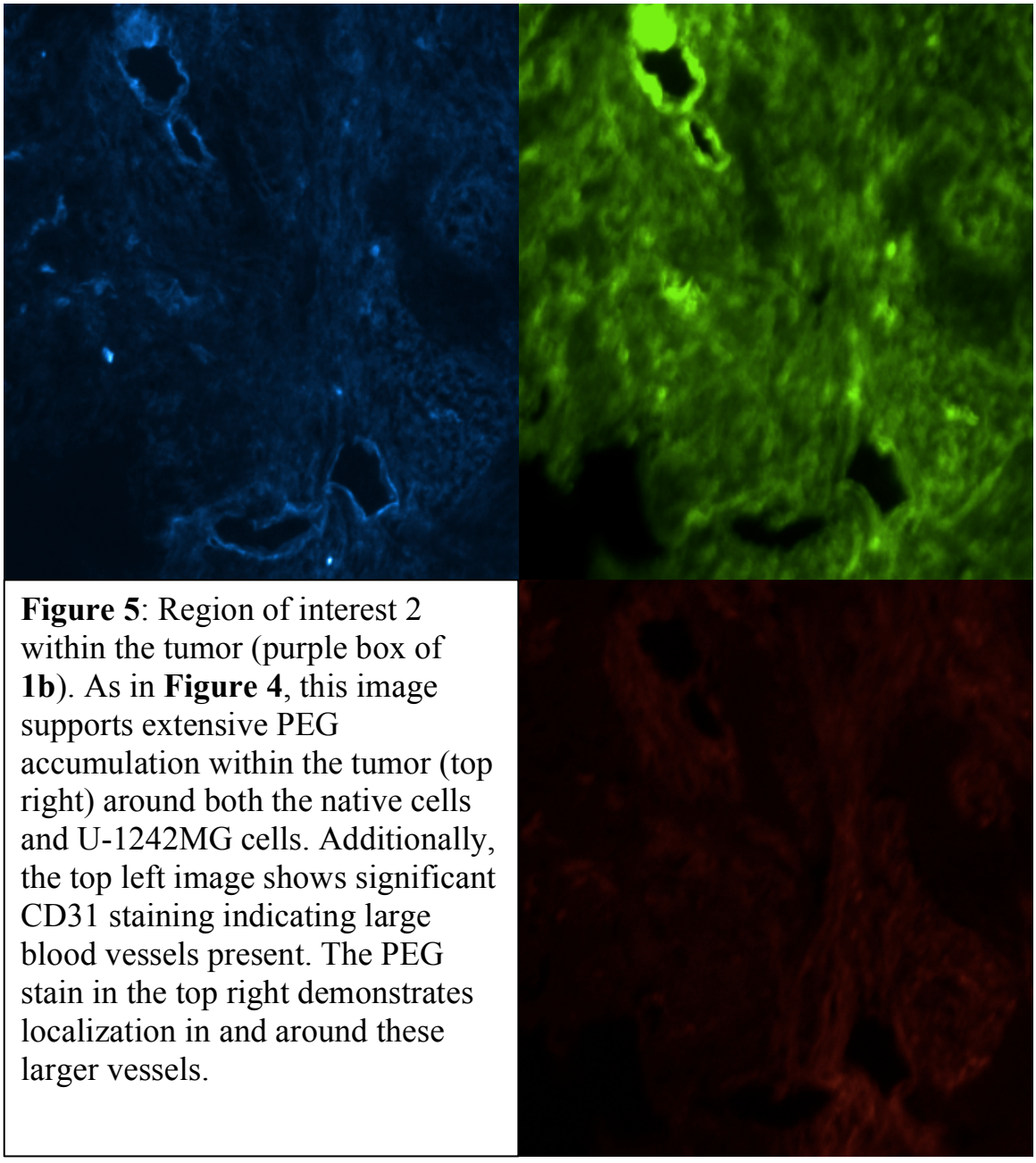

Figure 5: Region of interest 2 within the tumor (purple box of **1b**). As in **Figure 4**, this image supports extensive PEG accumulation within the tumor (top right) around both the native cells and U-1242MG cells. Additionally, the top left image shows significant CD31 staining indicating large blood vessels present. The PEG stain in the top right demonstrates localization in and around these larger vessels.

b. 10X Magnification Snaps:

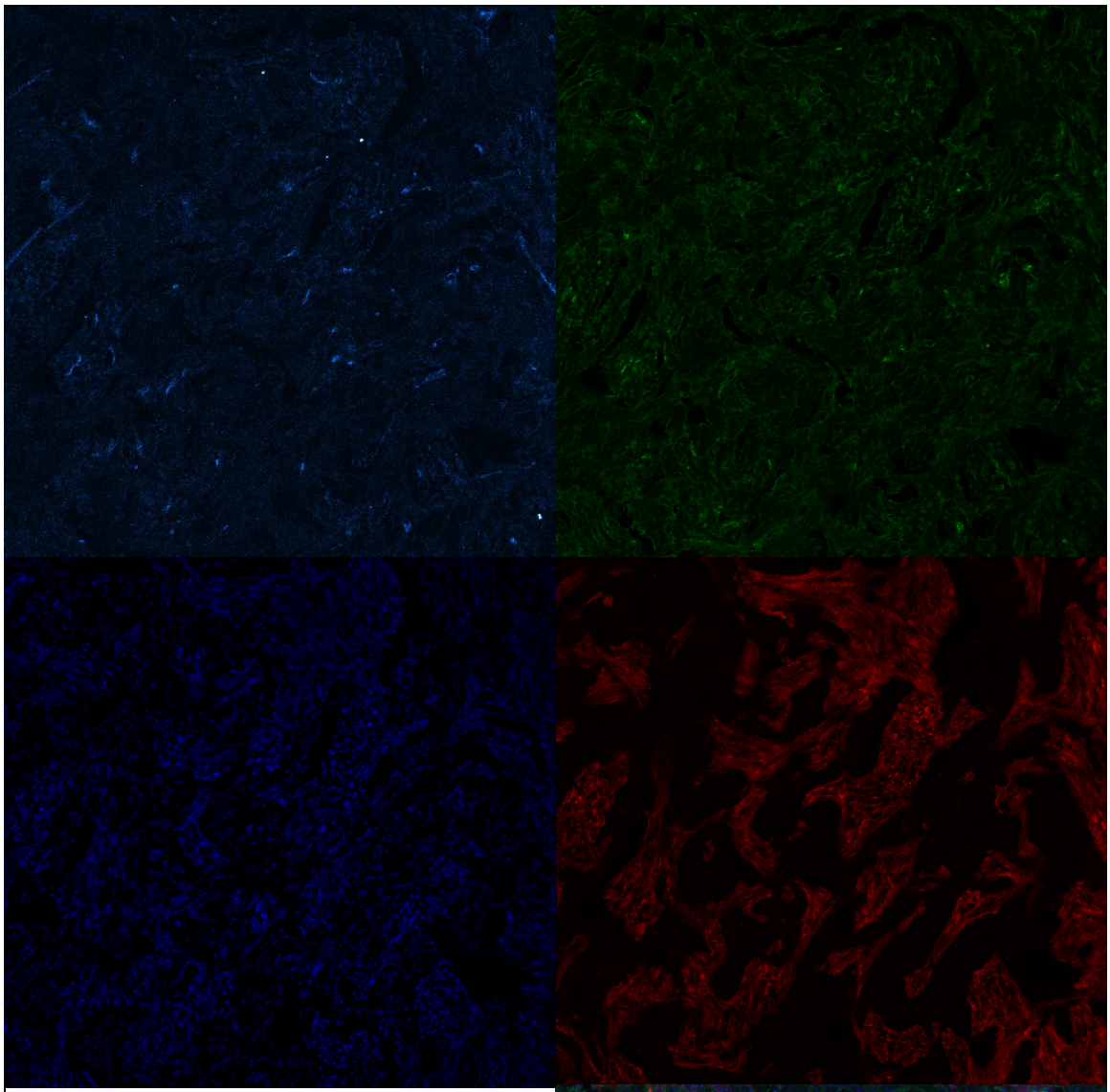

Figure 6: 10X magnification images of the tumor region showing CD31 (top left), nuclei (middle left), U-1242MG (middle right), and PEG (top right). Additionally, a composite image of all 4 channels is shown bottom right. These images show PEG in both healthy and cancerous tissue withing the tumor.

c. 63X Magnification Images:

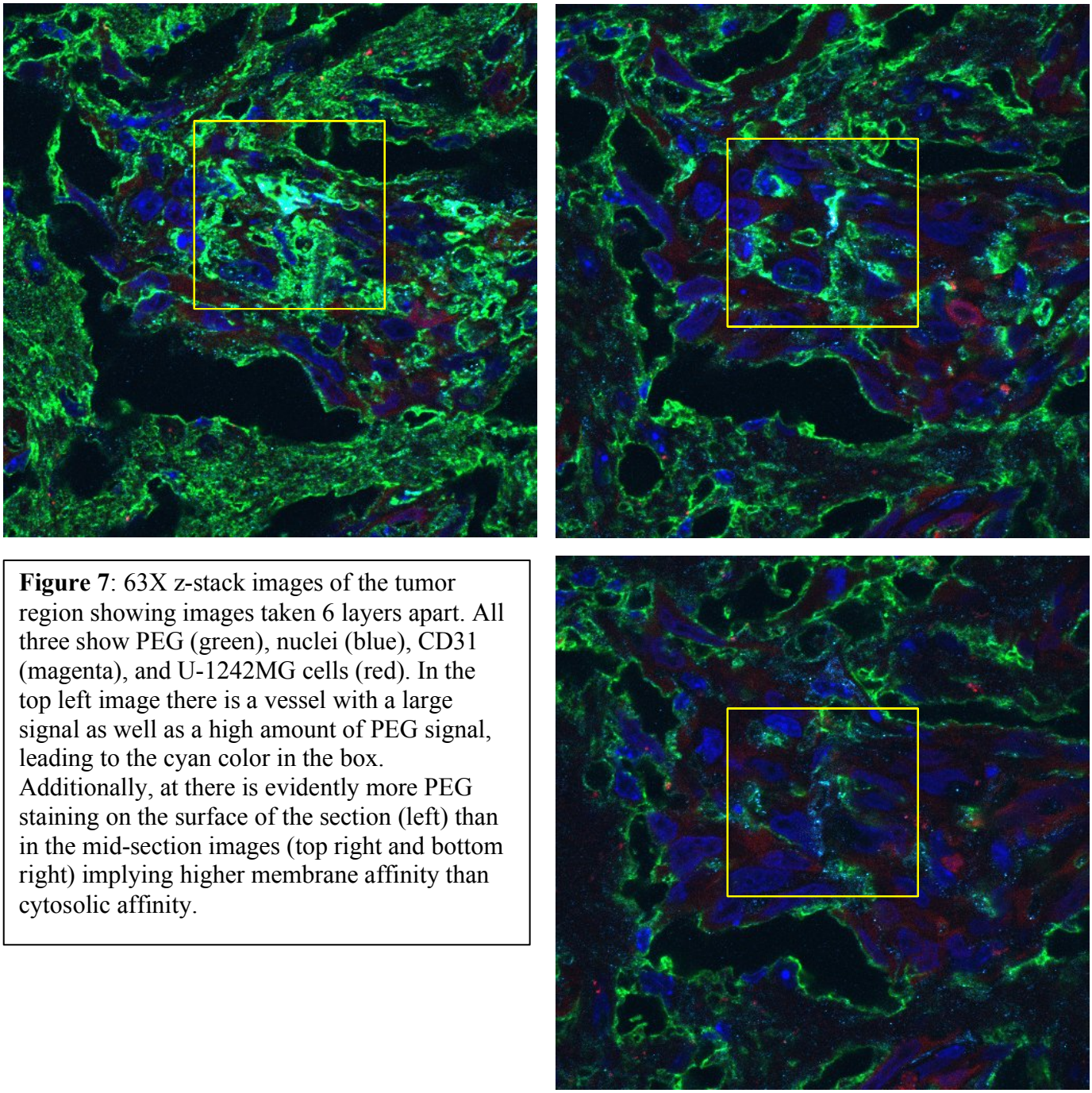

Figure 7: 63X z-stack images of the tumor region showing images taken 6 layers apart. All three show PEG (green), nuclei (blue), CD31 (magenta), and U-1242MG cells (red). In the top left image there is a vessel with a large signal as well as a high amount of PEG signal, leading to the cyan color in the box. Additionally, at there is evidently more PEG staining on the surface of the section (left) than in the mid-section images (top right and bottom right) implying higher membrane affinity than cytosolic affinity.

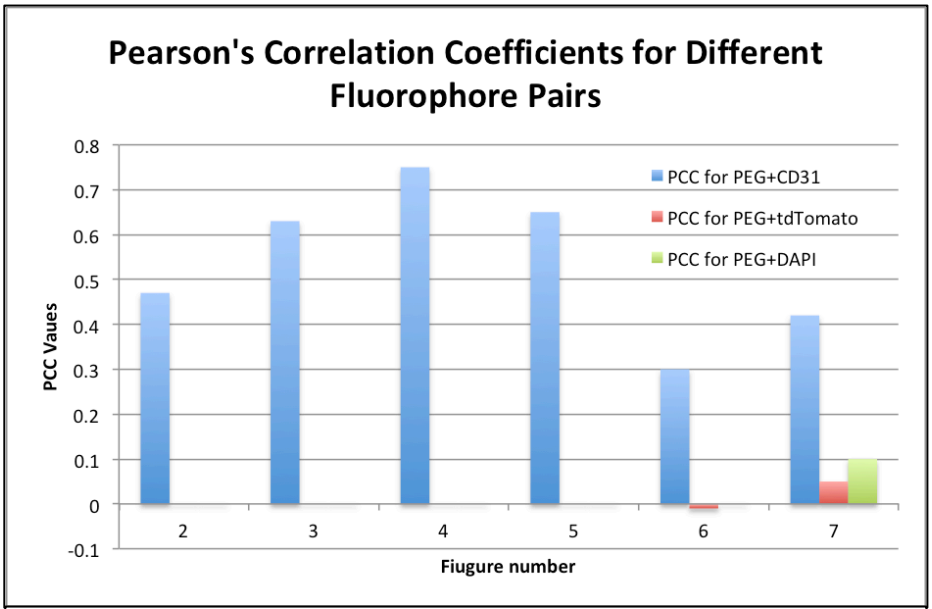

Chart 1: Pearson's Correlation Coefficients

V. Discussion:

The images presented in the results section contain qualitative information detailing the extent of tumor growth, the endothelial vascularization of the brain's tissues, including within the implanted tumor, and the location of the PEG within the brain as an indication of where the novel nanoparticles end up. All of this information is potentially useful to investigators interested in increasing the efficacy of nanoparticle related cancer therapies, and specifically radiation therapy. In particular, understanding the precise localization of the novel INPs is important because it can allow researchers to determine differences in treatment success based on nanoparticle localization. For example, it could allow researchers to discern differences in treatments utilizing INPs that localize in the membrane, cytosol, or the nucleus, and what phenomena allow for specific localization.

From the 10X images it is clear the PEGylated nanoparticles accumulate in the tumor region. This is a well-documented phenomenon called the enhanced permeability and retention (EPR) effect [13] of nanoparticles and other molecules and it is caused by the

presence of incomplete basal membranes and gaps in endothelial cells frequently present in tumor vasculature [19, 20]. Thus, regardless of the size of the PEG ligands on the INP, there is a strong propensity for nanoparticles to accumulate in the tumor interstitium, given they have enough time to circulate in the blood and eventually deposit there. Additionally, **Figure 6** supports the notion that once in the interstitium, the PEGylated INPs can translocate through diffusion or convection to noncancerous regions within the invasive tumor [19]. This is an especially important revelation in regards to determining the final efficacy of radiation therapy, because it demonstrates there is potential for the radiation dose enhancement of heavy atom based nanoparticles to also effect noncancerous tissue within a tumor.

One of the major pieces of evidence this research supports is the localization of the PEGylated nanoparticles on the exterior of groups of cells and in the voids between cells where tight junctions are not present. Additionally, the absence of the PEG signals within the cells, specifically in regions also expressing tdTomato, should be noted. This supports the conclusion that these INPs do not penetrate the cell in detectable quantities within 24 hours of the last INP injection. There are several possible explanations for this effect, with many relating to the PEG ligands on each INP. In order to increase the circulation time of the nanoparticles, PEG is attached because it is relatively hydrophilic for a hydrocarbon polymer, due to its polar ether linkages, allowing it to remain in the blood for longer periods. In addition, PEG often acts to mask the nanoparticles from non-specific cellular uptake by decreasing protein adsorption to the nanoparticle underneath, leading to an increase in specific cellular uptake if conjugated biomolecules are present and an increase in the amount of nanoparticles that eventually deposit in the interstitium of a tumor [14, 16, 17, 19]. PEG

also increases the hydrodynamic radius of the nanoparticle inhibiting renal excretion and allowing a further increase in circulation time.

Nonetheless, though the ligation of PEG to the INPs has the effect of potentially increasing the number of nanoparticles that may deposit in the tumor, it may also limit the amount that enters the cells via phagocytosis or pinocytosis. This is because the PEG coating inhibits protein adsorption and thus receptor-mediated endocytosis. Thus, PEGylated nanoparticles may become trapped in the interstitium and not permitted readily into the cells. Additionally, there is some evidence that if the INP is slightly ionic in character, the amphiphilic nature of the PEGylated INP may allow it to remain within cell membranes and resist passing into the cytosol [16].

The localization of the INPs in the vasculature of the brain both within and outside of the tumor region is supported in the images presented, especially in **Figure 2** and **Figure 3**. Though, the PEG signal is detectable when far from the tumor site, it is not nearly as widespread and does not exist as much outside of the vasculature as within the tumor region. Nonetheless, substantial deposition must occur in the vasculature as **Figure 3** supports, showing more complete vessels than the endothelial marker CD31 staining is capable of. This is evident because in the same region CD31 and PEG staining overlap, however PEG staining continues to mark the blood vessels while CD31 ceases to completely do so. This could be because more PEG molecules are present in these vessels at the surface exposed to the incubation fluid, where as CD31 is a protein used for intracellular junctions and thus may be secluded from the surface in many locations. Likewise, within the tumor region there is some evidence that supports the hypothesis that the INPs are localizing in the vasculature, however the CD31 staining is rather diffuse and many clear vessels are not always easy to

identify. Additionally, the vast presence of PEG signal in the tumor may mask some of the specificity of the accumulation within the tumor vasculature. It should also be noted that when the cells are implanted an injury is created leading to a small amount of bleeding. If this injury does not fully heal by the time the INP is injected, then there is a chance the injury can contribute to the wide distribution of INP within and around the tumor site.

Additionally, it is worth discussing the ordinary size of glioblastomas found in human brains and the proportional size presented in this study. In humans, glioblastoma tumors are most often found occupying a total of about 2 percent of the brain's entire volume. This is rather large and when projected into a mouse model corresponds to roughly 9 microliters of tumor volume out a total brain volume of 450 microliters. In this study, the cross section presented in the tile-scan image shows a tumor with an approximate average radius of 1.37 mm. If the tumor is assumed to be spherical in shape then the total volume of the tumor is roughly 10.8 microliters. This is slightly larger than the average but not by a great deal and thus the tumor could likely be expected to behave in a similar manner in regards to INP uptake. Also it should be noted that the U-1242MG cell line is a very invasive tumor and potential satellite tumors are possible in regions of the brain separated from the main tumor mass. If this occurs, the physical and chemical structure of the tumor microenvironments may be altered in more than one region of the brain leading to a potential increase in the overall INP retention. This is important because there could be regions of the imaged section affected by tumor cells not in the plane of the imaged section but in the same microenvironment.

Though this imaging study showed some clear results and evidence in support of where the novel INPs localize in murine brains implanted with U-1242MG tumors, there might

need to be more work performed in order to rule out several alternative explanations for the results obtained. First, in order to confirm or deny the conclusion that the INPs localize solely outside of the cells and do not penetrate the cell membrane, a staining protocol in which the cell membranes are made permeable to allow for intracellular immunostaining to be performed could be done. This could be done with permeabilizing molecules like saponin, Triton X-100, or Tween 20, that make either reversible or permanent holes in the cell membranes allowing both primary and secondary antibodies to diffuse through the cell membrane and attach to intracellular antigens, possibly including intracellular PEG [24].

Another factor that may obscure the results is that the endothelial marker protein CD31 (also known as PECAM1) used in this imaging is also expressed on the surfaces of many blood components including platelets and white blood cells, specifically monocytes, neutrophils and some T cells, though these mice lack T cells [25]. If these cells were able to exit the tumor via the leaky vasculature and remain in the interstitium, there could be non-specific staining occurring. If so, then within the tumor region it may be harder to detect blood vessels present and thus staining protocols with antibodies specific for platelet or white blood cell surface proteins could be used to confirm or deny their presence within a tumor, or a more specific endothelial cell marker could be selected such as CD34, CD54, CD45, VEGF-R2, vWF, Tek, or several others [26].

Lastly, the duration between when the mice received their INP injections and when the tissue was harvested could have a significant impact in the total uptake of the deposited INPs. In order to determine the uptake over time of the INP into the tumor cells, an experiment assessing the differences in cellular uptake of the INPs versus duration between injection and tissue harvesting could be performed.

VI. Conclusion:

Ultimately, through the use of both low-power and high-power conventional and confocal fluorescence light microscopy techniques, substantial preliminary evidence in the localization of novel Iodine-based nanoparticles within murine brains containing implanted human glioma U-1242MG tumors was obtained. This was done through the probing of the endothelial cell marker CD31, the tumor-expressed fluorescent protein tdTomato, and the INP conjugated poly(ethylene glycol), and their respective immunocytochemistry primary and secondary antibodies. Among such evidence was that the novel INPs from Nanoprobes Inc. localized primarily in and around the tumor region nearly uniformly throughout cancerous and noncancerous cells. Additionally, the INPs localized primarily in the brain's vasculature when found outside of the tumor region. There is also evidence that the INPs did not enter the cells in significant quantities but rather remained in the interstitium and along the exterior of cell clusters. In the end, though there are some additional procedures that can be performed to further confirm the results obtained, this evidence may still support further research into how these nanoparticles may be used in the treatment of cancer through radiation dose enhancement. Additional treatment methods including drug delivery, photothermal dose enhancement, and future nanoparticle based therapies and technologies may also benefit from this study.

VII. References:

1. Preusser, M. , de Ribaupierre, S. , Wöhrer, A. , Erridge, S. C., Hegi, M. , Weller, M. and Stupp, R. (2011), Current concepts and management of glioblastoma. Ann Neurol., 70: 9-21. doi:10.1002/ana.22425
2. Jaffray DA, Gospodarowicz MK. Radiation Therapy for Cancer. In: Gelband H, Jha P, Sankaranarayanan R, et al., editors. Cancer: Disease Control Priorities, Third Edition (Volume 3). Washington (DC): The International Bank for Reconstruction and Development / The World Bank; 2015 Nov 1. Chapter 14.
3. Baskar, R., Dai, J., Wenlong, N., Yeo, R., & Yeoh, K. (2014). Biological response of cancer cells to radiation treatment. Frontiers in Molecular Biosciences,1. doi:10.3389/fmolb.2014.00024
4. Buboltz JB, Dulebohn SC. Hyperbaric, Brain Radiation Necrosis. [Updated 2017 May 14]. In: StatPearls [Internet]. Treasure Island (FL): StatPearls Publishing; 2018 Jan-
5. Garbow, J. R., Tsien, C. I., & Beeman, S. C. (2018). Preclinical MRI: Studies of the irradiated brain. Journal of Magnetic Resonance. Retrieved April 26, 2018.
6. Santos, R, et al. "Radiation Dose Enhancement in Tumors with Iodine." *Medical Physics.*, U.S. National Library of Medicine, www.ncbi.nlm.nih.gov/pubmed/6843516.
7. Candelaria, Myrna, et al. "Radiosensitizers in Cervical Cancer. Cisplatin and Beyond."*Radiation Oncology*, BioMed Central, 8 May 2006, ro-journal.biomedcentral.com/articles/10.1186/1748-717X-1-15.
8. Hainfeld, J. F., Smilowitz, H. M., O'Connor, M. J., Dilmanian, F. A., & Slatkin, D. N. (2013). Gold nanoparticle imaging and radiotherapy of brain tumors in mice. Nanomedicine,8(10), 1601-1609. doi:10.2217/nnm.12.165
9. Hainfeld, J. F., Lin, L., Slatkin, D. N., Dilmanian, F. A., Vadas, T. M., & Smilowitz, H. M. (2014). Gold nanoparticle hyperthermia reduces radiotherapy dose. Nanomedicine: Nanotechnology, Biology and Medicine,10(8), 1609-1617. doi:10.1016/j.nano.2014.05.006
10. Arvizo, R., Bhattacharya, R., & Mukherjee, P. (2010). Gold nanoparticles: Opportunities and challenges in nanomedicine. Expert Opinion on Drug Delivery,7(6), 753-763. doi:10.1517/17425241003777010
11. ten Dam MA, Wetzels JF. Toxicity of contrast media: an update. Neth J Med. 2008; 66: 416-22.
12. Alkilany, A. M., & Murphy, C. J. (2010). Toxicity and cellular uptake of gold nanoparticles: what we have learned so far? Journal of Nanoparticle Research, 12(7), 2313–2333. http://doi.org/10.1007/s11051-010-9911-8
13. Barua, S., & Mitragotri, S. (2014). Challenges associated with penetration of nanoparticles across cell and tissue barriers: A review of current status and future prospects. Nano Today,9(2), 223-243. doi:10.1016/j.nantod.2014.04.008
14. PARAMBATH, A., & PARAMBATH, A. (2018). 13 – Stealth coatings for nanoparticles: Polyethylene glycol alternatives. In ENGINEERING OF

BIOMATERIALS FOR DRUG DELIVERY SYSTEMS: Beyond polyethylene glycol. S.l.: WOODHEAD.

15. Verhoef, J. J., & Anchordoquy, T. J. (2013). Questioning the use of PEGylation for drug delivery. Drug Delivery and Translational Research,3(6), 499-503. doi:10.1007/s13346-013-0176-5
16. Ahn, S., Seo, E., Kim, K., & Lee, S. J. (2013). Controlled cellular uptake and drug efficacy of nanotherapeutics. Scientific Reports,3(1). doi:10.1038/srep01997
17. Suk, J. S., Xu, Q., Kim, N., Hanes, J., & Ensign, L. M. (2016). PEGylation as a strategy for improving nanoparticle-based drug and gene delivery. Advanced Drug Delivery Reviews,99, 28-51. doi:10.1016/j.addr.2015.09.012
18. Salmaso, S., & Caliceti, P. (2013). Stealth Properties to Improve Therapeutic Efficacy of Drug Nanocarriers. Journal of Drug Delivery,2013, 1-19. doi:10.1155/2013/374252
19. Jain, R. K. (1987). Transport of molecules across tumor vasculature. Cancer And Metastasis Review,6(4), 559-593. doi:10.1007/bf00047468
20. McDonald, D. M., & Baluk, P. (2002, September 15). Significance of Blood Vessel Leakiness in Cancer. Retrieved from http://cancerres.aacrjournals.org/content/62/18/5381
21. Glioblastoma (GBM). (n.d.). Retrieved from http://www.abta.org/brain-tumor-information/types-of-tumors/glioblastoma.html
22. Oh, E., Delehanty, J. B., Sapsford, K. E., Susumu, K., Goswami, R., Blanco-Canosa, J. B., . . . Medintz, I. L. (2011). Cellular Uptake and Fate of PEGylated Gold Nanoparticles Is Dependent on Both Cell-Penetration Peptides and Particle Size. ACS Nano,5(8), 6434-6448. doi:10.1021/nn201624c
23. Calvo, P., Gouritin, B., Villarroya, H., Eclancher, F., Giannavola, C., Klein, C., . . . Couvreur, P. (2002). Quantification and localization of PEGylated polycyanoacrylate nanoparticles in brain and spinal cord during experimental allergic encephalomyelitis in the rat. European Journal of Neuroscience,15(8), 1317-1326. doi:10.1046/j.1460-9568.2002.01967.x
24. Jamur, M. C., & Oliver, C. (2009). Permeabilization of Cell Membranes. Immunocytochemical Methods and Protocols Methods in Molecular Biology,63-66. doi:10.1007/978-1-59745-324-0_9
25. PECAM1 platelet and endothelial cell adhesion molecule 1 [Homo sapiens (human)] - Gene - NCBI. (n.d.). Retrieved from https://www.ncbi.nlm.nih.gov/gene?Db=gene&Cmd=ShowDetailView&TermToSearch=5175
26. Endothelial cell markers. (2018, May 10). Retrieved from http://www.abcam.com/primary-antibodies/endothelial-cell-markers
27. Zhao, Y., Xiao, A., Dipierro, C. G., Carpenter, J. E., Abdel-Fattah, R., Redpath, G. T., . . . Hussaini, I. M. (2010). An Extensive Invasive Intracranial Human Glioblastoma Xenograft Model. The American Journal of Pathology,176(6), 3032-3049. doi:10.2353/ajpath.2010.090571

VIII. Acknowledgements:

I would like to thank the lab of Dr. Smilowitz for guiding and advising this project and making the imaging process possible through many hours of hard work implanting, monitoring, and explanting the tumors. In edition, I'd especially like to thank Sharif Ridwan for training me in many techniques and always making time to teach new concepts and information. Additionally, I would like to thank Dr. James Hainfeld and the rest of Nanoprobes Inc. for synthesizing and providing the novel Iodine-based nanoparticles used in this experiment. Lastly, I would like to thank Dr. McGuire and the entire Office of Undergraduate Research for making this research possible and assisting me along the way, as well as the Honors Department for making opportunity possible.